Article

Selective NO₂ Gas Sensors Employing Nitrogen- and Boron-Doped and Codoped Reduced Graphene Oxide

Chiheb Walleni, Shuja Bashir Malik, Ghada Missaoui, Mohamed Ayoub Alouani, Mohamed Faouzi Nsib, and Eduard Llobet*
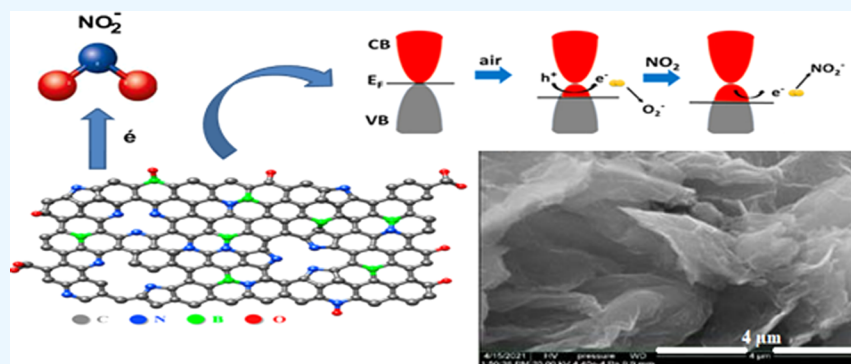
Read Online

| ACCESS | | Metrics & More | | Article Recommendations | | SI Supporting Information |

ABSTRACT: In this paper, we develop high-performance gas sensors based on heteroatom-doped and -codoped graphene oxide as a sensing material for the detection of NO₂ at trace levels. Graphene oxide (GO) was doped with nitrogen and boron by a chemical method using urea and boric acid as precursors. The prepared samples were characterized by scanning electron microscopy (SEM), transmission electron microscopy (TEM), Raman spectroscopy, X-ray diffraction (XRD), and X-ray photoelectron spectroscopy (XPS). The obtained results proved the successful reduction of graphene oxide by doping effects, leading to the removal of some oxygen functional groups and restoration of an sp² carbon structure. New bonds in honeycombs, such as pyridinic, pyrrolic, graphitic, B−C₃, B−C₂−O, and B−O, were created. Compared to the nondoped GO, the N/B-rGO materials exhibited enhanced responses toward low concentrations of NO₂ (<1 ppm) at 100 °C. Particularly, the N-rGO-based device showed the highest sensitivity and lowest limit of detection.

1. INTRODUCTION

In recent decades, chronic lung diseases have increased their prevalence and become responsible for a high number of premature deaths worldwide. Their impacts are caused by the respiration of toxic gases, especially NO₂, NO, CO, and SO₂.[1] To protect human health and monitor our environment, it is therefore important to detect trace amounts of these gases.[2] Specifically, the development of NO₂ gas sensors has been the subject of numerous research studies, aiming to find a typical sensing material that accomplishes a good response time, enhanced selectivity, high sensitivity, and low limit of detection.

A complementary metal oxide semiconductor (CMOS) is a technology for developing low-power integrated circuits. It finds application in various domains, including analog circuits like image sensors, data converters, RF circuits, and highly integrated transceivers designed for diverse communication methods.[3] In this context, integrating 2D materials (e.g., graphene) with CMOS technology offers tremendous potential for significantly enhancing chip functionality and enabling the emergence of 2D applications that match the complexity of the

devices. Moreover, the unique advantages of these materials, including large surface area and versatile modulation methods, offer remarkable performance advantages compared to existing technologies at the device level.[4]

Metal oxides, including ZnO, NiO, and SnO₂, have often been the preferred choice for developing gas sensors due to their favorable characteristics, such as wide band gap, high stability and sensitivity, and inexpensiveness.[5−7] However, some challenges affect their gas detection performance, such as poor selectivity, high operating temperature (and associated high energy consumption), and also complex preparation methods.[8−10] These challenges limit the application of metal oxides for NO₂ sensing. Otherwise, conducting polymers have
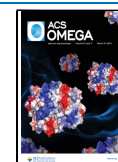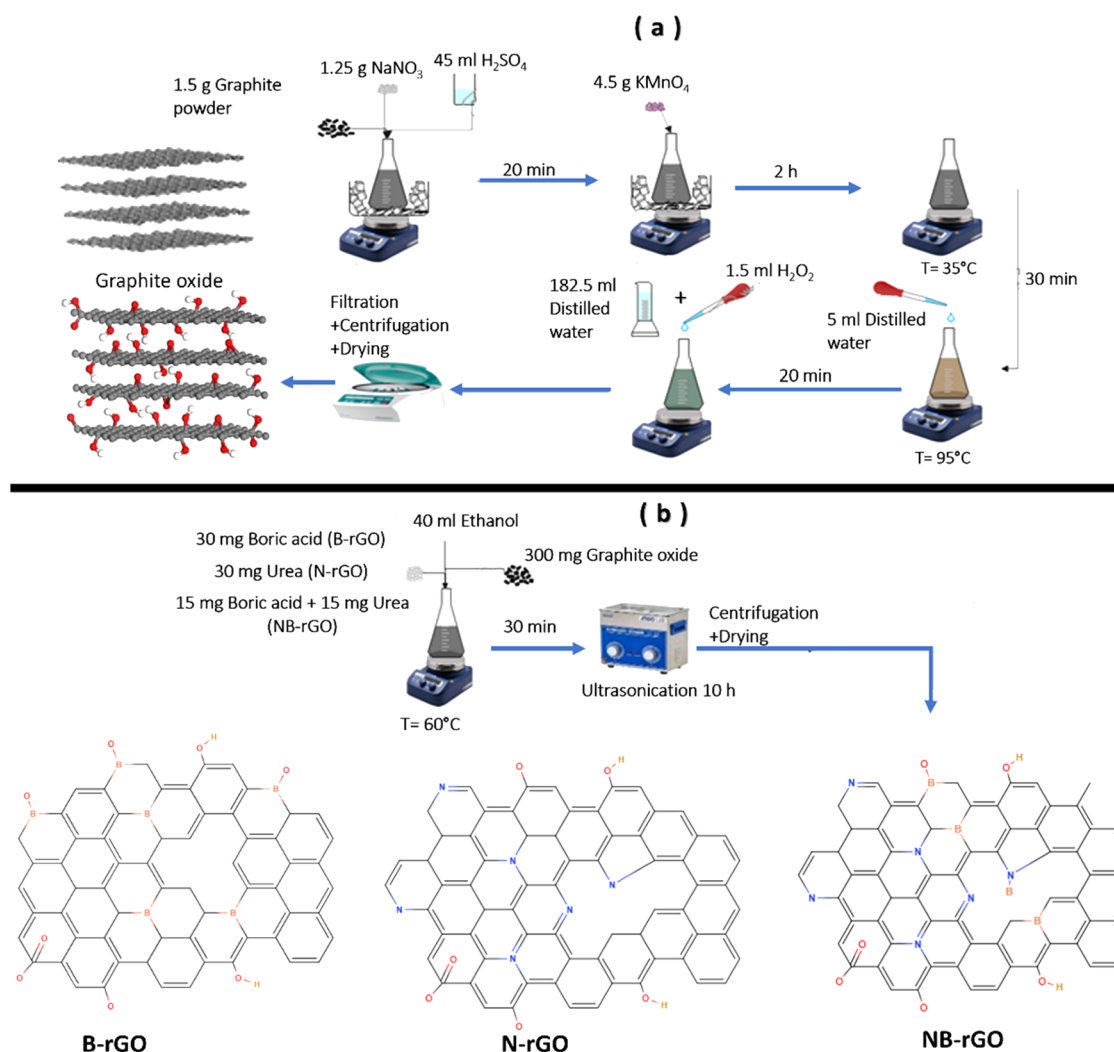
Figure 1. Synthesis process of (a) graphite oxide and (b) N-rGO, B-rGO, and NB-rGO. Adapted with permission from *Small* 2017, 13, 1701835. Copyright 2017, Wiley.

also been the subject to many studies[11,12] as gas-sensitive materials, but their performance and marketability have been somewhat limited because they suffer from important moisture cross-sensitivity and undergo degradation processes when operated under ambient conditions.

Alternatively, graphene-based materials were suggested in the past decade to substitute metal oxides and conducting polymers in gas sensing applications. Graphene materials show advantages, such as being produced using cost-effective methods, transparency, and superior corrosion resistance, and possess unique properties, such as high conductivity and high surface area.

Graphene was first produced and identified by Geim and Novoselov in 2004 at the University of Manchester.[13,14] It is a single layer of graphite with a thick sheet of sp^2-bonded carbon atoms arranged in a honeycomb lattice.[15] This carbon-based nanomaterial has attracted the interest of many researchers due to its outstanding and unique properties in various fields, such as energy storage, electronics, and organic solar cells.[16−20] Moreover, graphene-based gas sensors have emerged as promising candidates for reaching the market due to their excellent features, such as 2D-like structure (high surface area 2629 $m^2 \cdot g^{-1}$) and high carrier mobility.[20,21] Nevertheless, despite all of these good properties, pristine graphene is not

well suited as a gas-sensitive nanomaterial because of its chemical inertness and lack of active sites for the physisorption or chemisorption of gas molecules.[20,22]

On the other hand, graphene oxide (GO) is a nanomaterial derived from graphene, which contains a large number of active sites owing to the presence on its surface of oxygen-containing functions, such as hydroxyl, epoxy, and carbonyl groups. These oxygenated functionalities are responsible for the higher reactivity of GO.[23,24] Several research studies have been dedicated to the application of GO and heteroatom-doped GO in the field of gas sensors. Prezioso and co-workers[23] developed a NO$_2$ sensor based on the GO film and showed that the sensor became inactive when operating temperatures exceeded 200 °C due to the poor thermal stability of GO. Besides, the sensitivity was weak at a low concentration of NO$_2$. On the other hand, GO-based sensors showed a high adsorption of H$_2$O molecules due to their strong hydrophilic behavior attributed to the presence of oxygen functional groups.[25] However, the introduction of oxygen-containing active sites on graphene results in significant damage to its conjugated π-structure and leads to a sharp decrease in electrical conductivity. Accordingly, as the NO$_2$ sensing mechanism is based on its adsorption on active sites and associated charge transfer processes, it is therefore needed

to balance the electrical conductivity and the surface reactivity when developing a new material for NO_2 sensing.

One of the most promising approaches for improving the surface reactivity without decreasing the electrical conductivity is chemical doping of graphene networks with heteroatoms like B, N, P, and S.[26−28] Therefore, chemically doped GO can be regarded as a promising candidate for an efficient NO_2 sensor. Either by surface transfer or substitution of carbon atoms in the graphene lattice, doping with heteroatoms affects graphene's surface, chemical, and electronic characteristics, as well as its free charge carrier densities and electrical conductivity.[29]

Lv et al.[30] investigated boron-doped graphene to examine its ability to detect NO_2 and NH_3 at low concentrations. Also, Shaik et al.[31] studied nitrogen-doped graphene sheets for the detection of NO_2 at low concentrations and found a limit of detection of about 2.5 ppm. Dai and co-workers[32] presented a theoretical study using density functional theory (DFT) on gas adsorption by graphene doped with boron, nitrogen, aluminum, and sulfur. They found that graphene doped with B and S was more sensitive to polluting gases, such as NO and NO_2. Esrafili[33] also performed a theoretical study on boron- and nitrogen-codoped graphene for NO, NO_2, and CO gas detection and showed that doping graphene changes its electronic behavior and increases the interaction between gas molecules and the graphene surface.

Accordingly, the aim of this research is to explore a straightforward and inexpensive route for the N and/or B doping of GO as a way to achieve doped reduced graphene oxide (rGO). The use of doped rGO for developing highly sensitive and selective chemoresistive NO_2 sensors is then investigated and performance is compared against that of pristine GO sensors.

The main structure and properties of the prepared samples were studied using different techniques, such as scanning electron microscopy (SEM), transmission electron microscopy (TEM), X-ray diffraction (XRD), Raman spectroscopy, and X-ray photoelectron spectroscopy (XPS). The sensing films were deposited on alumina transducing substrates by airbrushing as an easy preparation method, and then, sensors were exposed to different gas concentrations while operated at room temperature and at 100 °C. Gas sensing results are discussed together with sensing mechanisms.
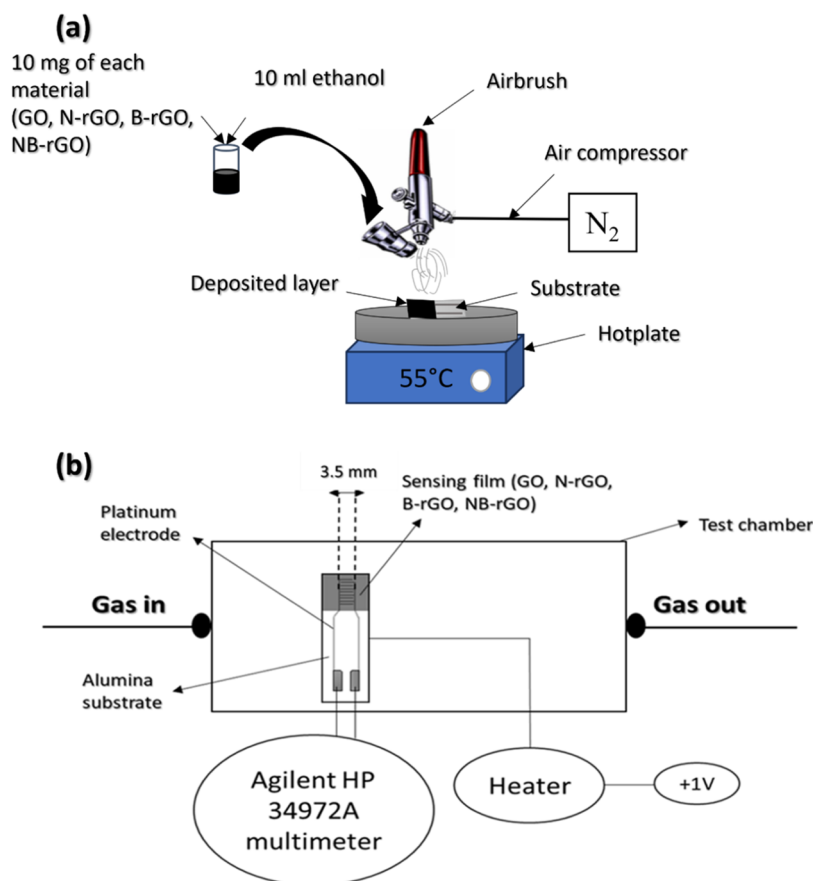
2. EXPERIMENTAL SECTION

2.1. Synthesis of Graphite Oxide. Following the modified Hummers method[34,35] (Figure 1a), 1.5 g of natural graphite powder and 1.25 g of $NaNO_3$ were mixed in 45 mL of a concentrated H_2SO_4 (95−98%) solution and kept under vigorous stirring for 20 min in a beaker immersed in an ice bath. Then, 4.5 g of $KMnO_4$ was added carefully to the mixture and the stirring was maintained for 2 h. In the process of oxidizing graphene, the reaction involves permanganate anions. These anions play a role in the oxidation of graphite by introducing oxygen-based groups like epoxides, hydroxyls, and carboxyls. After that, the ice bath was removed, and the solution was stirred at 35 °C for 30 min. Afterward, 5 mL of distilled water was added slowly, the reaction temperature rose abruptly to 95 °C, and the color of the mixture turned brown. After 20 min of stirring at 95 °C, 182.5 mL of distilled water was added to the mixture, and the heating was turned off. The suspension was further treated by adding 1.5 mL of hydrogen peroxide (30%), giving the mixture a green color. After that,

the mixture was filtered, washed several times with distilled water, and then dried at 80 °C overnight to obtain the graphite oxide powder free from unreacted chemicals and manganese side products.

2.2. Synthesis of Graphene Oxide and B/N-Doped and -Codoped Reduced Graphene Oxide (rGO). Initially, 0.250 g of graphite oxide powder was stirred in 40 mL of distilled water for 30 min and ultrasonicated for 1 h to obtain a graphene oxide (GO) suspension. To prepare each of the doped rGO (B-rGO and N-rGO), we proceeded as follows (Figure 1b): 0.250 g of graphite oxide powder was stirred in 40 mL of distilled water for 30 min and ultrasonicated for 1 h to obtain graphene oxide (GO) suspension. Subsequently, 10 mL of ethanol solution of urea/boric acid (3 mg·mL^{-1}) was added to the previously prepared GO solution. Urea and boric acid were utilized as the nitrogen (N) and boron (B) sources, respectively. Additionally, the incorporation of N and B dopants was intended to facilitate the reduction of graphene oxide. The mixture was subjected to magnetic stirring for 30 min at a temperature of 60 °C and then to ultrasonication for 10 h at a temperature of 80 °C. Finally, the product was filtered and washed with distilled water several times and dried in the oven overnight at 80 °C. The same procedure was carried out to prepare the codoped reduced graphene oxide (NB-rGO), using a solution containing 1.5 mg·mL^{-1} urea and 1.5 mg·mL^{-1} boric acid as the precursor source.

2.3. Material Characterization. The morphology of samples was investigated through scanning electron microscopy (SEM) using a Quanta 450 from FEI. Additionally, transmission electron microscopy (TEM) images were acquired using an ultrahigh-resolution transmission electron microscope (UHR-TEM)—Libra 200MC. Structural characterization involved X-ray diffraction (XRD) patterns obtained through a Shimadzu Corporation-LabX XRD-600 instrument with Cu Kα copper anticathode radiation (λ = 1.54056 Å). The recording was conducted at room temperature within the 2θ range 10−80°, with steps of 0.05° and an accumulation time of 20 s/step. Raman spectra spanning a wavelength range of 100−3000 cm^{-1} were obtained using a Raman spectrometer (Renishaw inVia Raman Microscope). The laser used had a wavelength of 532 nm. Furthermore, X-ray photoelectron spectroscopy (XPS) was performed using a PHI 5000 VersaProbe photoelectron spectrometer (Ulvac-PHI, Inc., Chikasaki, Japan). Surface analysis by XPS involved irradiating the material with monoenergetic soft X-rays of Mg Kα (1253.6 eV). The energy resolution was 0.6 eV. A dual-beam charge neutralization system consisting of an electron gun (∼1 eV) and an argon ion gun (<10 eV) was used to compensate for built-up charge during the measurements. All XPS binding energies were calibrated to the Au 4f$_{7/2}$ peak at 84.0 eV.

2.4. Sensing Layer Preparation and Measurements. The preparation of sensing devices was performed by dispersing 10 mg of each material (GO, N-rGO, B-rGO, or NB-rGO) in 10 mL of ethanol under agitation for 30 min. The suspension was further ultrasonicated for 1 h and then deposited on platinum screen-printed electrodes (alumina substrates from CeramTech GmbH) by the airbrushing technique at a temperature range of 55−60 °C.[36] During electrode coating, the film resistance was monitored using a multimeter. This approach enabled enhancement of the device-to-device reproducibility. The thickness of the deposited sensing layers was 50 ± 5 μm. N_2 was used as the carrier

Figure 2. (a) Sensor preparation and (b) systematic experimental setup for performing measurements. Adapted with permission from *J. Alloys Compd.*, 2023, 941, 169011. Copyright 2023, Elsevier.

gas for the airbrushing process. The sensor preparation process is illustrated in Figure 2a.

The fabricated sensors were placed inside an airtight Teflon test chamber with a volume of 35 cm^3 and tested both at room temperature and at 100 °C (Figure 2b). To optimize the system power consumption and enable operation under more realistic test conditions, the total flow rate was adjusted to a low rate of 100 mL/min. The gas sensing measurements were carried out after stabilization of the fabricated sensors under synthetic dry air for 30 min. Subsequently, sensors were exposed for 10 min to the target gas diluted with synthetic dry air. Throughout the whole measurement phase, the temperature inside the test chamber was 25 °C and there was a remnant ambient humidity (4% R.H.), which corresponds to about 1250 ppm water vapor. An Agilent HP 34972A multimeter was used to measure the resistance values of the sensors. Sensor response, R (%), was defined as follows:

$$R \ (\%) = [(R - R_0)/R_0] \times 100$$

where R_0 is the resistance under dry air and R is the resistance value obtained under each exposure to the target gas.

3. RESULTS AND DISCUSSION

3.1. Morphological Analysis. The morphology of the prepared samples was observed by using a scanning electron microscope (SEM). Figure 3a shows the SEM image of GO. The surface morphology of GO consists of many agglomerated and wrinkled sheets, often found in fully oxidized to GO,[37−39] allowing the presence of oxygenated functional groups. After

doping and codoping with boron and nitrogen, as depicted in Figure 3b−d, the appearance of the materials at the scale shown was almost identical to that of GO and was not affected by the ultrasonication step. The observed wrinkles and corrugations might also be ascribed to the intercalation of boron and nitrogen within the graphene.[40,41]

The surface morphology of the prepared samples was further examined by using TEM. The results, shown in Figure 4, confirmed the flake-type nanostructure of the prepared doped and undoped GO samples. The dark spots indicate a thick stacking nanostructure of several layers of graphene oxide, while the transparent areas suggest much thinner films of few layers.[34,42−44] Selected area electron diffraction (SAED) patterns, shown in Figure 4a−d, present well-defined spot patterns composed of extended bright spots in a hexagonal configuration. This corresponds to rGO in the [001] axis area.[45] Nevertheless, electron diffraction of N-rGO and NB-rGO films forms a ring-shaped diffraction pattern with scattered bright spots. This is an indication that the crystalline graphene sheets are partially disoriented in the N-doped graphene caused by the structural distortions induced by the intercalation of N atoms.[45] Moreover, the TEM image of the NB-rGO material shows a porous sheet-like structure confirmed by the observed corrugations (Figure 4d). This structure favors electrocatalysis applications because the active sites can be exposed to reactant molecules, particularly NO$_2$ and other gas molecules.[46] Thus, the NB-codoped reduced graphene oxide can facilitate electron transport during the redox process and improve the electrocatalytic activity.[26]
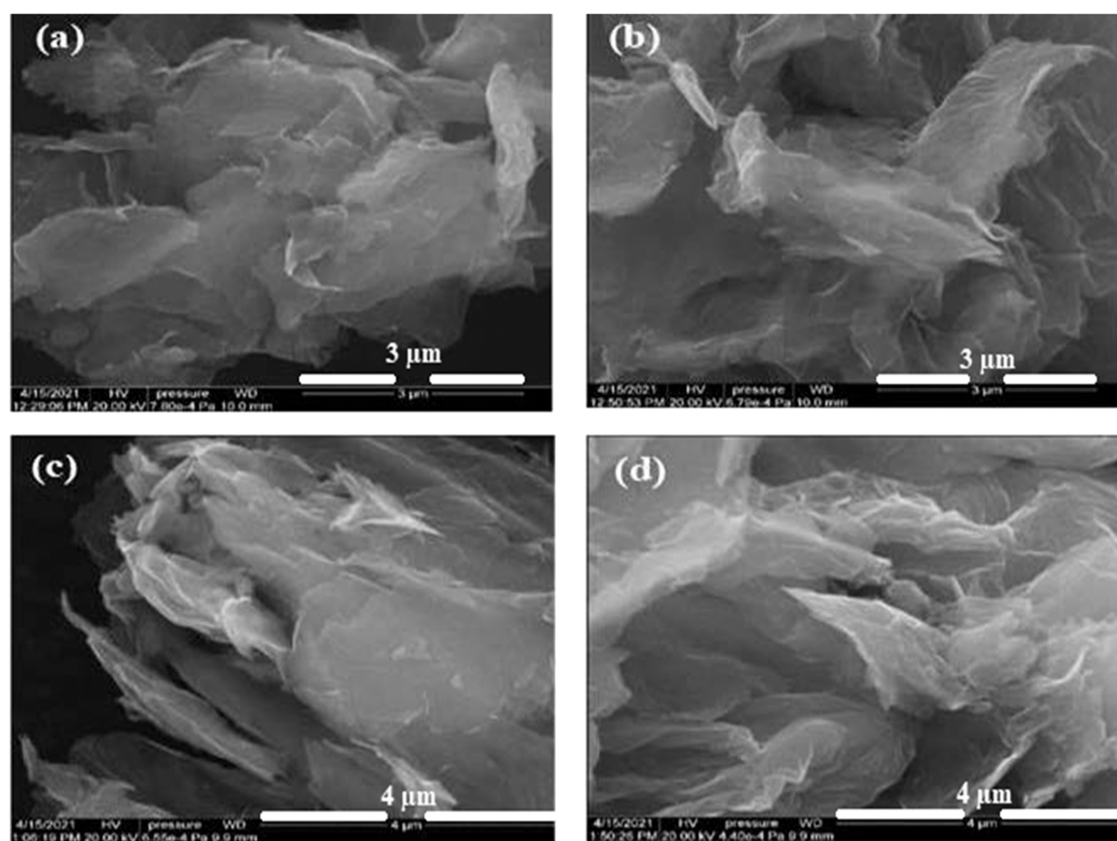
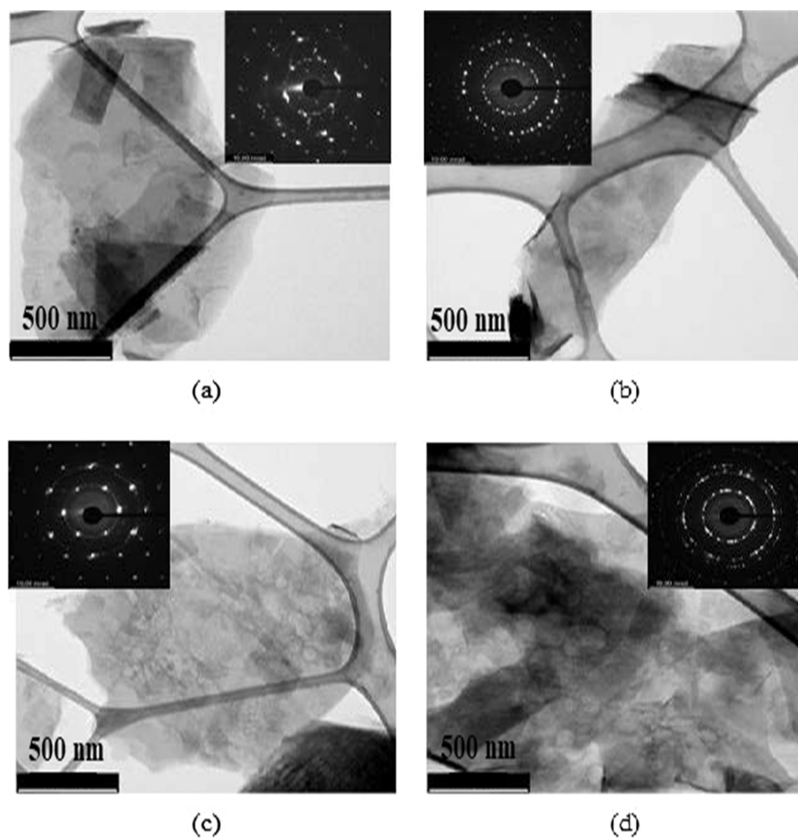**Figure 3.** SEM images of (a) GO, (b) N-rGO, (c) B-rGO, and (d) NB-rGO.

Figure 4. TEM image and SAED pattern of (a) GO, (b) N-rGO, (c) B-rGO, and (d) NB-rGO.
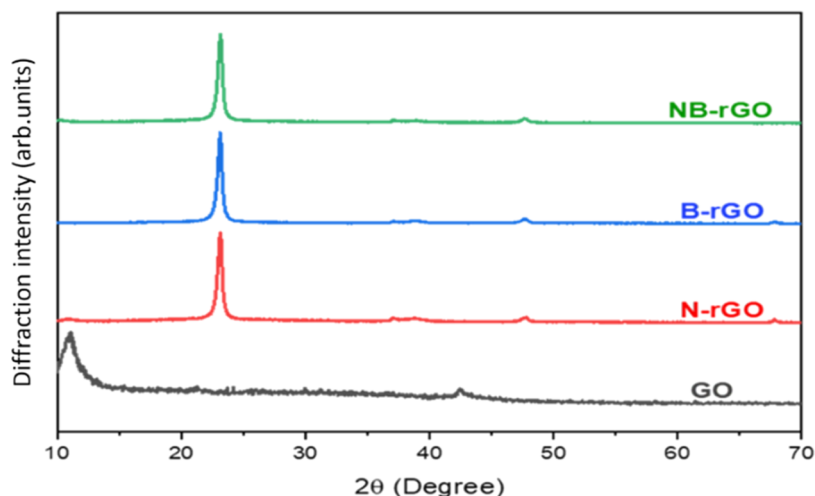
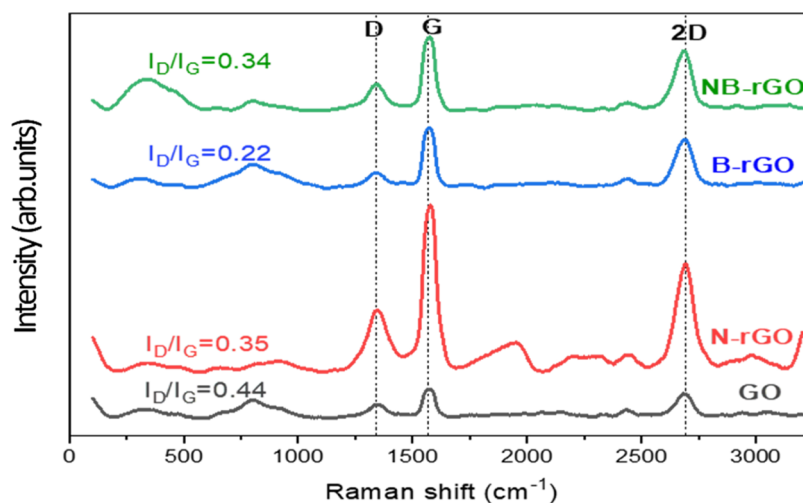**Figure 5.** XRD diagrams of GO, N-rGO, B-rGO, and NB-rGO.

Figure 6. Raman spectra of GO, N-rGO, B-rGO, and NB-rGO.

3.2. XRD Analysis. The crystal structure of the prepared samples (GO, N-rGO, B-rGO, and NB-rGO) was examined by XRD analysis (Figure 5). The diffractogram of GO displays a broad peak at about $2\theta = 11°$ (001). This peak is indicative of the presence of oxygen functional groups in the GO structure subsequent to the oxidation of graphite.[47] Nevertheless, this distinctive peak of GO vanishes completely in the XRD pattern of N-rGO, B-rGO, and NB-rGO samples; and a new characteristic peak appears at 23.13° (002) for the last three samples. This means that most of the oxygen-containing groups in GO were efficiently eliminated after the reduction and doping with heteroatoms.[41] This also indicates that the π-conjugated structure of graphene has been restored considerably at the produced rGO. Similar XRD profiles have been reported by Abid et al.[48]

The small intensity peak observed at $2\theta = 43°$ (100) in the XRD diffractogram for GO corresponds to the honeycomb structure formed by sp²-hybridized carbons. Additionally, a similar intensity peak appears in N-rGO, B-rGO, and NB-rGO at $2\theta = 48°$, which is also attributed to the same structure. It should be taken into account that the 2θ value can shift due to the introduction of dopants, such as N and B. The presence of these dopants may induce defects in graphene, leading to the

creation of defect sites and structural disruptions in the carbon lattice, ultimately resulting in lower crystallinity.[49]

The distance between two layers is a crucial characteristic for determining the structural information on the material.[50] The interlayer spacing (d-spacing) can be calculated using Bragg's Law:

$$2d \cdot \sin\theta = n\lambda$$

where n is an integer, λ is the wavelength of Cu Kα as 1.541 Å, d is the interlayer spacing of the crystal planes (Å), and θ is the Bragg angle.

The decrease in the d-spacing value reveals that the GO has been significantly reduced by the removal of oxygen functional groups in its structure.[51] Moreover, doping with heteroatoms is expected to create defects in the rGO structure making d-spacing changes.[48] Indeed, the d-spacing in the GO sample is found to be $d = 0.803$ nm, but it decreased to an average of $d = 0.384$ nm in B-rGO, N-rGO, and NB-rGO samples, indicating both the successful incorporation of boron and nitrogen atoms into the GO layer and also the removal of most oxygen functional groups on the GO surface.[41]

3.3. Raman Spectroscopy. Figure 6 represents the Raman shifts of GO, N-rGO, B-rGO, and NB-rGO. The as-made electrocatalysts present a common D band at 1339 cm⁻¹, G
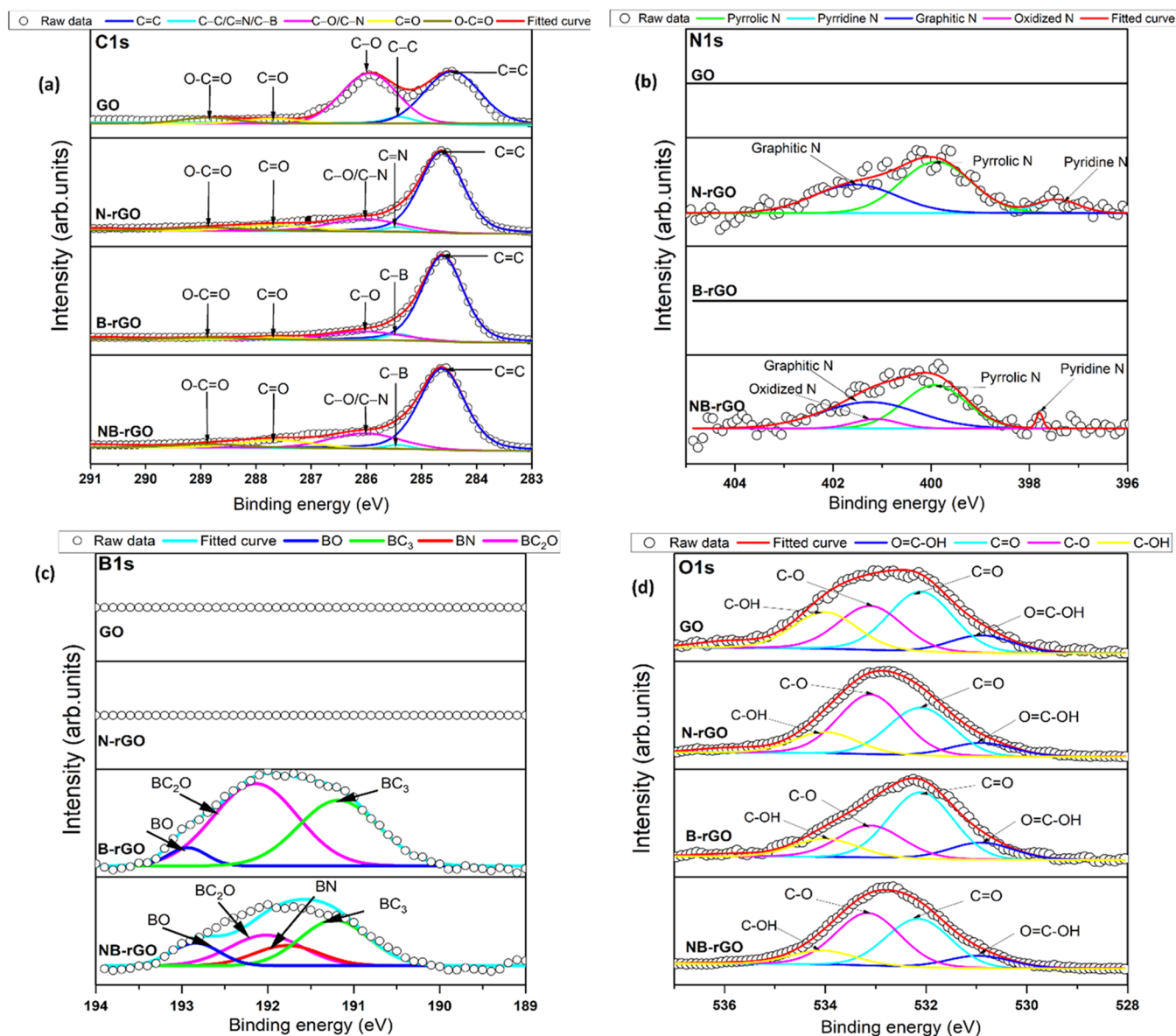
Figure 7. High-resolution deconvoluted C 1s (a), N 1s (b), B 1s (c), and O 1s (d) XPS spectra for GO and B/N-doped and -codoped rGO samples.

band at 1570 cm^{-1}, and a 2D band at 2690 cm^{-1}. The D line is associated with the vibrations of carbon atoms with dangling bonds in disordered graphite planes and the defects incorporated into pentagon and heptagon graphite-like structures. The G band is caused by the first-order scattering of the E$_{2g}$ phonon of sp^2 C atoms at the Brillouin Zone center and is present in all sp^2 bonds in a graphitic network. It represents the structural intensity of the sp^2-hybridized carbon atom.[52] The intensity of the G line is much greater and the width is thinner compared with that of the D line. The position of the G band was not changed upon the B/N doping, as expected and reported by Beams et al.[53] This behavior can be explained by the low concentration of dopants. Moreover, the position of the 2D band at 2690 cm^{-1} shows a multilayer structure of all of the samples since the monolayer nanostructure is usually observed at 2679 cm^{-1}.[54] More precisely, referring to the works of Ferrari et al.,[55,56] the position of the observed 2D band indicates that the number of

graphene layers can be estimated to be lower than 10, confirming the nanostructure of all of the samples.

The intensity ratio (I_D/I_G) indicates the quality of the material and the related concentration of sp^3 defects in the sp^2-hybridized graphene structure.[57] The intensity ratios of D (disorder) and G (graphitic) bands (I_D/I_G) of GO, N-rGO, B-rGO, and NB-rGO are 0.44, 0.35, 0.22, and 0.34, respectively. These results indicate that the GO sample has more dominant defect contents, likely due to abundant carboxylic, hydroxylic, and epoxy groups, expected to be distributed both in the bulk and at the edges in the graphene oxide sheets. However, the defects in GO are reduced as the sp^2 domains can be partially recovered by reduction and B/N doping. Such a self-healing phenomenon could be attributed to the insertion of N and B atoms in the crystal structure of rGO, which substituted the sp^3 C defect sites in the form of pyridinic N, quaternary N, pyrrolic N, and BC$_3$ and subsequently converted them to the sp^2 C form.[58] This behavior was more noticed when B was used as the dopant.

Nevertheless, the values of I_D/I_G also show that some defects persist in the B/N-rGO samples. These defects are suggested to be localized mainly along the edges and not in the basal plane of the graphene sheets.

3.4. XPS Analysis. To evaluate the elemental composition and chemical environment, X-ray photoelectron spectroscopy (XPS) measurements were performed.

Figure S2 shows the XPS survey spectra, which revealed the presence of C and O elements in all samples, N in N-rGO, B in B-rGO, and both N and B elements in NB-rGO. Table S1 lists the elemental compositions (in %) derived from the XPS component intensities.

High-resolution core-level XPS spectra of B1, C1, N1, and O 1s were acquired for inspecting the chemical environment of B, C, N, and O atoms of the prepared samples. Since the B 1s and N 1s peaks are of low intensities, they were amplified to be deconvoluted. The parameters used for the fitting of the XPS spectra are summarized in the Supporting Information (Table S2).

By curve fitting, the C 1s XPS spectrum (Figure 7a) reveals five components in all samples. The dominant component at 284.5 eV is attributed to the sp^2 carbon atoms (C=C), indicating that the majority of C atoms are structured in a honeycomb lattice.[58] The sp^3 C−C, C−O, C=O, and O=C−O chemical groups are represented by the other four low-intensity components centered at 285.3, 285.9, 287.6, and 288.8 eV, respectively. However, the C 1s spectrum of graphene oxide reveals prominent peaks corresponding to both C=C and C−O bonds.[59] Particularly, in the C 1s spectrum of B/N-doped rGO, both peaks attributed to C−C and C−O can also be assigned to C−B and C−N bonds, respectively.[60]

The high-resolution N 1s spectrum was used to identify the chemical states of various kinds of N dopants. As shown in Figure 7b, the N 1s spectrum for the N-rGO sample can be deconvoluted by three components. The component centered at 397.7 eV refers to nitrogen in the pyridine ring, the component at 399.9 eV indicates the presence of nitrogen atoms in the pyrrole ring, and the component at 401.6 eV corresponds to quaternary nitrogen atoms. In the N 1s spectrum of boron- and nitrogen-codoped graphene, an additional component attributed to oxidized O−N species appeared at 401.7 eV. Within graphene layers, graphitic N refers to N atoms replacing C atoms.[59] These findings show that nitrogen atoms were efficiently doped into the graphitic layer of reduced graphene oxide.

The deconvoluted B 1s spectrum corresponding to the B-rGO sample is shown in Figure 7c. The chemical bond for BC_3, which refers to the substitution of C atoms by B atoms in the graphene lattice, was found at 191.2 eV. The component at 193.1 eV could be tentatively attributed to the BC_2O structure, which contains a boron atom connected to one oxygen atom and two carbon atoms. The possible formation of B−O bonds is shown by the peak at 192.9 eV. The B 1s peak for the boron- and nitrogen-codoped reduced graphene oxide (NB-rGO) sample is deconvoluted into four components, namely, BC_3 (B-substituted C), B−N, BC_2O, and B−O centered at 191.2, 191.8, 192.0, and 192.8 eV, respectively.[40]

The O 1s peak for the GO sample, as shown in Figure 7d, consists of four different chemically shifted components and can be deconvoluted into the following: =C−OH (530.8 eV), C=O (532.0 eV), C−O (533.1 eV), and C−OH (534.0 eV). For N-rGO, the presence of oxygenated functions is observed as O=C−OH (530.7 eV), C=O (532.1 eV), C−O (533.1 eV), and C−OH (534.0 eV) groups.[61] The XPS O 1s spectrum of B-rGO can be curve-fitted into four components centered at about 530.1, 532.1, 533.2, and 534.0 eV attributable to the O=C−OH, C=O, C−O, and C−OH species, respectively.[62] In the O 1s spectrum of NB-rGO, the four peaks are observed. These peaks at 530.7, 532.1, 533.2, and 534.0 eV are assigned to O=C−OH, C=O, C−O, and C−OH.[63]

Considering the B 1s and O 1s XPS spectra, the presence of B_2O_3 (as it shares the same binding energy as BC_2O) cannot be ruled out.[60]

The XPS analyses suggest that GO, upon thermal annealing with boric acid and urea, contains boron and nitrogen functional groups as well as oxygen functional groups that remained after the oxidation of graphite.

3.5. Doping Effect in Graphene Oxide Electronic Properties. The introduction of boron (B) and nitrogen (N) atoms into graphene oxide is a logical choice owing to their similar atomic sizes compared to carbon (C) and their respective roles as hole acceptors and electron donors in substitutional B and N doping. From a theoretical standpoint, the electronic properties of graphene oxide are altered after the doping process. Following oxidation, graphene oxide develops a band gap, rendering it effectively insulating with a position of Fermi level in the valence band (Figure 8a).[64] Upon
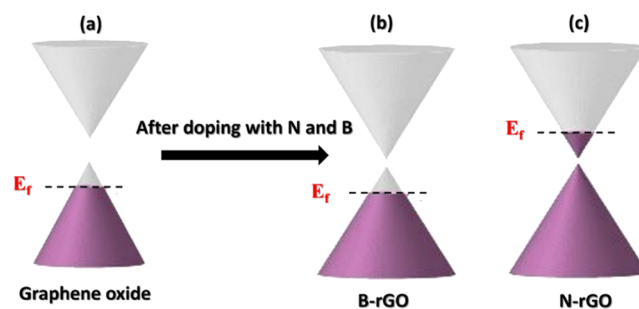
Figure 8. Electronic structure bands of (a) graphene oxide, (b) B-rGO, and (c) N-rGO.

substitutional doping with B and N atoms and subsequent reduction of certain oxygen functional groups, the band gap diminishes, leading to a significant enhancement in electrical conductivity. Consequently, the Fermi level is positioned in the valence and conduction bands, illustrating desirable p-type and n-type conducting electronic properties, as depicted in Figure 8b,c.[65]

3.6. Gas Sensing Measurements. The gas sensing characteristics of the prepared devices were evaluated by monitoring their relative resistance changes upon exposure to a specific concentration of NO_2. The gas detection measurements were carried out at room temperature, 100 °C, and 200 °C after applying different concentrations of NO_2: 100, 300, 500, 700, and 1000 ppb. When operated at room temperature, the different sensors showed a slight resistance change (not presented here), which could not be clearly distinguished from the noise signal. In addition, the NO_2 detection test at 200 °C showed either no response from GO, N-rGO, and B-rGO or a faint response from the NB-rGO-based sensors (see Figure S1). These NO_2 concentrations are at least 3 orders of magnitude lower than the one of background humidity (i.e., ~1250 ppm). However, when operated at 100 °C, responses were observed, indicating that a significant increase in

temperature could activate more active sites on the material surface for the adsorption of gas species.[66]

The repeatability of four sensors was evaluated by exposing the sensors to different concentrations of NO_2 for three consecutive sensing cycles at 100 °C. The four sensors have shown different baselines at the first cycle. The baseline resistance of the four sensors is not fixed and can change sinusoidally before being exposed to target gas, and it suggests that the baseline resistance is influenced by factors, such as environmental conditions and the sensor's internal dynamics. However, the second and third cycle displayed good repeatability and stability of 4 sensors.

Accordingly, it is clearly observed that GO-, B-rGO-, N-rGO-, and NB-rGO-based sensors displayed resistance changes toward consecutive pulses of NO_2 concentrations when operated at 100 °C (Figure 9).
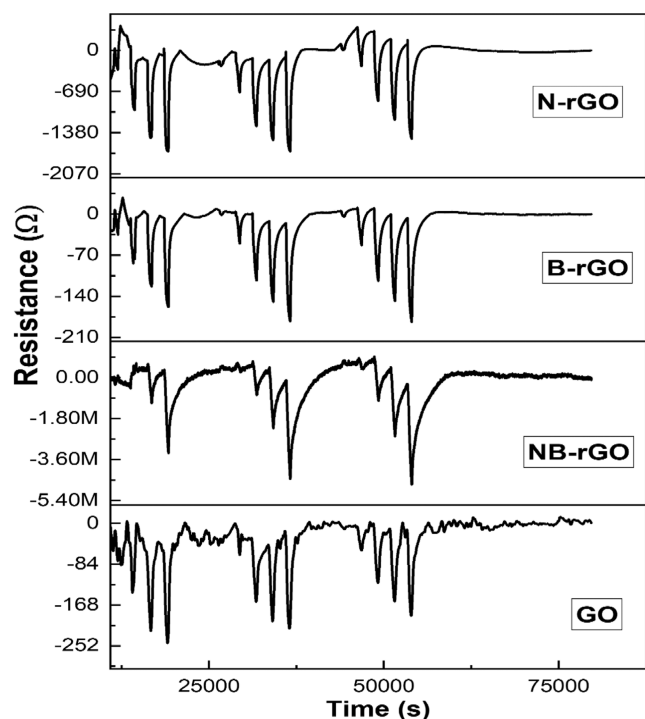
Figure 9. Repeatable cycles of 4 sensors. A linear baseline correction was applied to the response curves in view of minimizing drift.

Thus, a progressive increase in the responses of the four prepared sensors was observed according to the increase in the NO_2 concentration (Figure 10a). The four sensors displayed a good response to recovery time about $T_{resp}/T_{rec} = 10/30$ min. Likewise, the response of the GO-based sensor increased from 0.25 to 4.28% when the NO_2 concentration increased from 100 ppb to 1 ppm, while the B-rGO (NB-rGO, respectively) sensor showed a response increase from 0.33% (0.83%) to 4.73% (8.44%, respectively). Particularly, the N-rGO-based device displayed the highest response and the highest change in its response with the NO_2 concentration, which has boosted from 1.33% (at 100 ppb) to 11.8% (at 1 ppm). Moreover, the obtained results showed that the B-rGO, N-rGO, and NB-rGO-based sensors revealed a better response than the pristine GO, which proves the effect of doping in the improvement of the detection process.[67,68] This improvement may be related to the higher interaction existing between the doped GO surface (as showed by the XPS analysis) and NO_2 molecules, which

leads to a modification of the charge carrier concentration and hence to a change in the resistance of the films.[69] This occurs despite the surface of the doped GO encloses only few sites of oxygenated groups and sp^3 bonds,[23] usually expected to enhance the GO/NO_2 interaction. The reason for such a behavior is 2-fold: (i) the first is the morphological differences existing between doped and nondoped GO samples, as explained by Kacem et al.[70] The SEM images showed that doped GO samples are more exfoliated, thus presenting a more active surface to interact with NO_2 molecules than GO samples; (ii) the second is the conduction type, where it should be noted that the B/N-reduced graphene oxide samples display enhanced n-type conduction, which leads to the increased response in the presence of NO_2 molecules. Indeed, the rGO usually shows a p-type semiconductor material behavior. As an element of the fifth group, nitrogen further enhances the n-type conduction in rGO, which is located in graphene basal as pyrrolic, pyridinic, and graphitic bonds. Consequently, the nitrogen provides excess electrons that favor more interactions with NO_2. This process is consistent with findings by Chang et al. in the context of NO gas.[71] On the other hand, boron usually enhances the p-type conduction within the distribution of BC_3 and BC_2-OH bonds. This enhancement effectively boosts the p-type conduction of reduced graphene oxide (rGO) and may consequently facilitate the adsorption of NO_2 gas.[72] For the NB-rGO material, it enhances the n-type conduction mainly due to the presence of nitrogen.[33]

Figure 10b displays the calibration curves corresponding to NO_2 sensing by the prepared GO and doped rGO-based sensors. Table 1 shows the sensitivity and the limit of detection of each sensor, where the sensitivity is given by the slope of the calibration curve. The limit of detection can be calculated according to the formula:

$$LOD = 3 \times \frac{RMS_{noise}}{b}$$

where b is the slope of the calibration curve (sensitivity) and RMS_{noise} is the root-mean-square deviation at the baseline.[73]

It is clearly noticeable that the N-rGO-based sensor displayed the low LOD of 12 ppb and the highest sensitivity $(1171 \times 10^{-2} \text{ ppm}^{-1})$.

Additionally, a new evaluation of the four sensors was conducted for their response to alternative chemical gases with consistent concentrations, including NO_2 (1 ppm), ethanol (10 ppm), CO (100 ppm), and benzene (10 ppm; refer to Figure 11) at 100 °C. Notably, the 4 sensors exhibited an extreme selectivity specifically toward NO_2, relative to the other tested gases. This significant selectivity is particularly observed in the N-rGO sensor, which is attributed to the distinctive adsorption characteristics of NO_2.

These performances of the B/N-doped rGO are found to be better than those reported for graphene-based sensors (see Table S3) even though our measurements were carried out at lower NO_2 concentrations (i.e., ≤1 ppm). Accordingly, the synthesized B/N-doped rGO, and specifically, the N-rGO, is presented as a potential candidate with good NO_2 sensing properties.

A possible mechanism for the detection of NO_2 using B/N-rGO is proposed and illustrated in Figure 12.

The atmospheric oxygen molecules are adsorbed at the surface of graphene, where they are reduced to O_2^- and O^{2-} ions.[20] As illustrated in Figure 12, the capture of electrons by
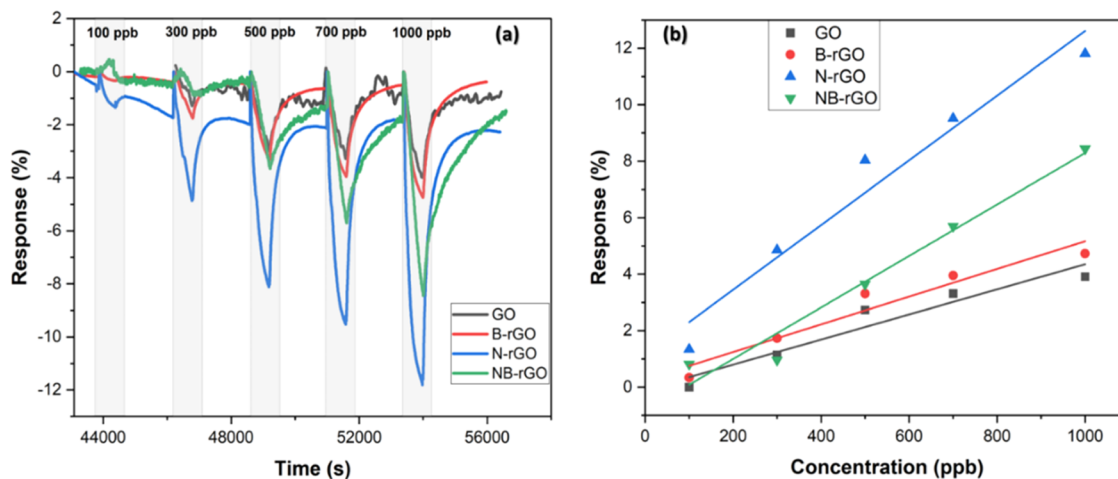
Figure 10. NO$_2$ response of GO, B-rGO, N-rGO, and NB-rGO at 100 °C (a) and associated calibration curves (b).

Table 1. Sensor Sensitivity and LOD Values

| sensors	GO	B-rGO	N-rGO	NB-rGO
sensitivity (10^{-2} ppm^{-1})	475	490	1171	909
LOD (ppb)	39	27	12	24

oxygen molecules leads to the shift of the Fermi level of graphene toward the valence band side. As oxidizing entities, NO$_2$ molecules also withdraw electrons from the graphene surface and oxygenated groups derived from GO and B/N-doped rGO. Similarly, the N atom can bind with one oxygen atom of the NO$_2$ molecule as confirmed by Adjizian et al.[74] Consequently, the Fermi level of the prepared graphene materials shifts further to the valence band, which results in more holes becoming available in the valence band, thus leading to a drastic decrease in sensor resistance upon exposure to nitrogen dioxide.[5,75] When NO$_2$ is removed from the sensor environment, the original equilibrium of surface species is regained, the Fermi level is shifted toward the conduction band, and the electrical resistance of the sensor increases to the baseline value in air (see Figure 9).

4. CONCLUSIONS

In summary, we have successfully synthesized boron- and nitrogen-doped and -codoped reduced graphene oxide using a simple chemical doping method. The prepared samples were widely investigated for their main structure and analyzed using SEM, TEM, XRD, Raman, and XPS techniques. Interestingly, boron and nitrogen dopants have been extremely involved in the reduction of graphene oxide by the removal of significant oxygen functional groups, as confirmed by the characterization results. In addition, NO$_2$ sensing devices based on the prepared samples were developed using a simple and inexpensive technique. Accordingly, B/N-rGO samples have proved higher performances for NO$_2$ sensing than the nondoped graphene oxide. This is suggested to be attributed to the distribution of active sites and created bonds, which effectively favors the transfer of electrons between NO$_2$ molecules and the graphene surface. Specifically, the N-rGO sensor has shown a higher response, sensitivity, and lower limit of detection than the other doped B-rGO and NB-rGO sensors toward NO$_2$ when operated at 100 °C. The created pyrrolic, pyridinic, and graphitic bonds are responsible for the enhanced n-type conduction, which is strongly related to the improved response
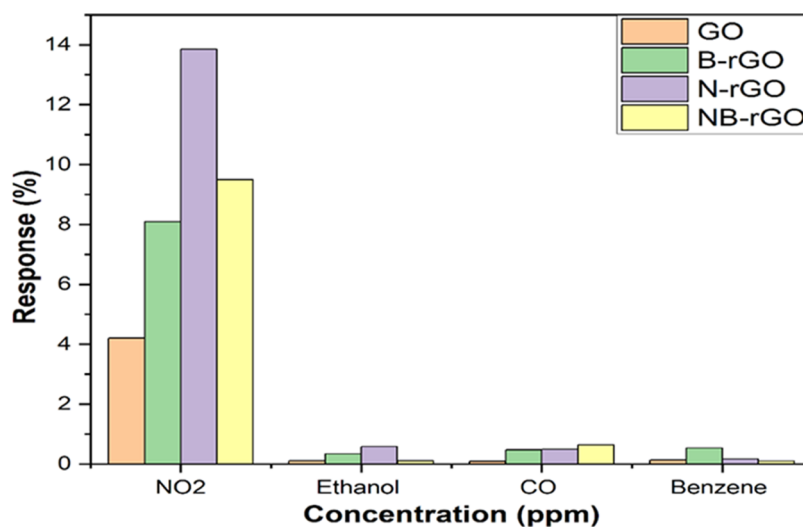
Figure 11. Responses of the 4 sensors to NO$_2$ (1 ppm), ethanol (10 ppm), CO (100 ppm), and benzene (10 ppm) at 100 °C.
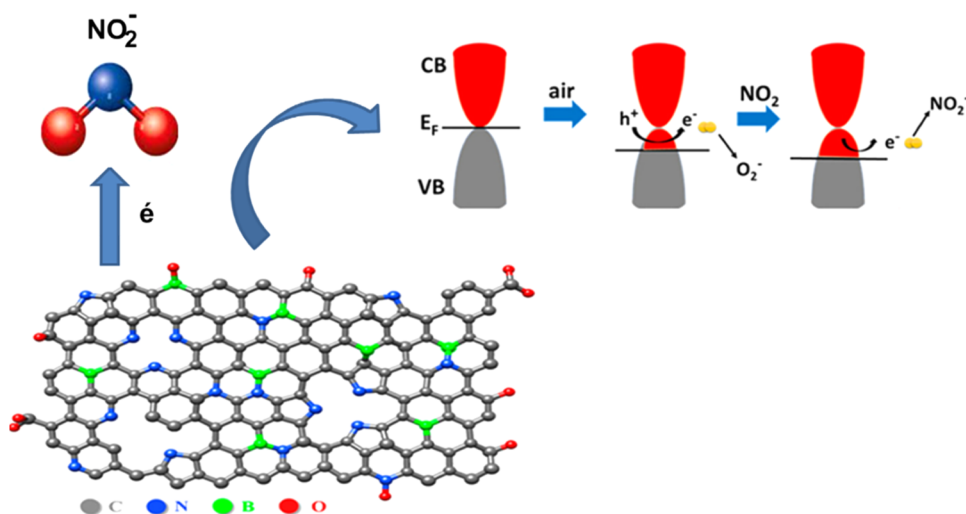
Figure 12. Proposed NO_2 sensing mechanism with the B/N-rGO-based sensor.

of the N-rGO sensor. Sensor performance could be optimized further by carefully tuning the N doping level of rGO, something easily achievable employing the synthesis method described here. This would be the subject of future research.

■ ASSOCIATED CONTENT

Ⓢ Supporting Information

The Supporting Information is available free of charge at https://pubs.acs.org/doi/10.1021/acsomega.3c09460.

> Figures showing the responses to nitrogen dioxide for the different sensors operated at 200 °C; Figure with the XPS survey spectra for the different samples analyzed; Table showing the chemical composition for the different samples; Table summarizing the parameters used for fitting the XPS data; Table enabling the comparison of the sensing performance achieved to the one of previously published works. (PDF)

■ AUTHOR INFORMATION

Corresponding Author

Eduard Llobet − MINOS, Universitat Rovira i Virgili, 43007 Tarragona, Spain; ⓞ orcid.org/0000-0001-6164-4342; Email: eduard.llobet@urv.cat

Authors

Chiheb Walleni − Higher School of Sciences and Technology of Hammam Sousse, University of Sousse, 4011 Sousse, Tunisia; MINOS, Universitat Rovira i Virgili, 43007 Tarragona, Spain; NANOMISENE Laboratory, LR16CRMN01, Center of Research on Microelectronics and Nanotechnology (CRMN), Technopole of Sousse, 4054 Sousse, Tunisia

Shuja Bashir Malik − MINOS, Universitat Rovira i Virgili, 43007 Tarragona, Spain

Ghada Missaoui − Fakultät V − Institute of Physics, Carl von Ossietzky Universität Oldenburg, D-26111 Oldenburg, Germany

Mohamed Ayoub Alouani − MINOS, Universitat Rovira i Virgili, 43007 Tarragona, Spain

Mohamed Faouzi Nsib − Higher School of Sciences and Technology of Hammam Sousse, University of Sousse, 4011 Sousse, Tunisia; NANOMISENE Laboratory, LR16CRMN01, Center of Research on Microelectronics and Nanotechnology (CRMN), Technopole of Sousse, 4054 Sousse, Tunisia

Complete contact information is available at:
https://pubs.acs.org/10.1021/acsomega.3c09460

Notes

The authors declare no competing financial interest.

■ REFERENCES

(1) Wu, D.-W.; Chen, S.-C.; Tu, H.-P.; Wang, C.-W.; Hung, C.-H.; Chen, H.-C.; Kuo, T.-Y.; Wang, C.-F.; Lai, B.-C.; Chen, P.-S.; Kuo, C.-H. The Impact of the Synergistic Effect of Temperature and Air Pollutants on Chronic Lung Diseases in Subtropical Taiwan. *J. Pers. Med.* **2021**, *11*, 819.

(2) Wu, J.; Wu, Z.; Han, S.; Yang, B.-R.; Gui, X.; Tao, K.; Liu, C.; Miao, J.; Norford, L. K. Extremely Deformable, Transparent, and High-Performance Gas Sensor Based on Ionic Conductive Hydrogel. *ACS Appl. Mater. Interfaces* **2019**, *11*, 2364−2373.

(3) Filipovic, L.; Selberherr, S. In *Integration of Gas Sensors with CMOS Technology*, 4th IEEE Electron Devices Technology & Manufacturing Conference (EDTM), 2020; pp 1−4.

(4) Lemme, M. C.; Akinwande, D.; Huyghebaert, C.; Stampfer, C. 2D Materials for Future Heterogeneous Electronics. *Nat. Commun.* **2022**, *13*, No. 1392.

(5) Yang, S.; Jiang, C.; Wei, S. Gas Sensing in 2D Materials. *Appl. Phys. Rev.* **2017**, *4*, No. 021304.

(6) Saruhan, B.; Lontio Fomekong, R.; Nahirniak, S. Review: Influences of Semiconductor Metal Oxide Properties on Gas Sensing Characteristics. *Front. Sens.* **2021**, *2*, No. 657931.

(7) Wang, C.; Yin, L.; Zhang, L.; Xiang, D.; Gao, R. Metal Oxide Gas Sensors: Sensitivity and Influencing Factors. *Sensors* **2010**, *10*, 2088−2106.

(8) Dey, A. Semiconductor Metal Oxide Gas Sensors: A Review. *Mater. Sci. Eng. B* **2018**, *229*, 206−217.

(9) Nikolic, M. V.; Milovanovic, V.; Vasiljevic, Z. Z.; Stamenkovic, Z. Semiconductor Gas Sensors: Materials, Technology, Design, and Application. *Sensors* 2020, 20, 6694.

(10) Uma, S.; Shobana, M. K. Metal Oxide Semiconductor Gas Sensors in Clinical Diagnosis and Environmental Monitoring. *Sens. Actuators, A* 2023, 349, No. 114044.

(11) Steffens, C.; Brezolin, A. N.; Steffens, J. Conducting Polymer-Based Cantilever Sensors for Detection Humidity. *Scanning* 2018, 2018, 4782685.

(12) Bai, H.; Shi, G. Gas Sensors Based on Conducting Polymers. *Sensors* 2007, 7, 267−307.

(13) Geim, A. K.; Novoselov, K. S. The Rise of Graphene. *Nat. Mater.* 2007, 6, 183−191.

(14) Novoselov, K. S.; Andreeva, D. V.; Ren, W.; Shan, G. Graphene and Other Two-Dimensional Materials. *Front. Phys.* 2019, 14, No. 13301.

(15) Geim, A. K. Graphene: Status and Prospects. *Science* 2009, 324, 1530−1534.

(16) Latif, U.; Raza, M. A.; Rehman, Z. U.; Iqbal, J.; Lee, N.; Mehdi, S. M. Z.; Maqsood, M. F.; Hussain, S. Binder Free Heteroatom-doped Graphene Oxide as High Energy Density Electrodes for Supercapacitor Applications. *Int. J. Energy Res.* 2022, 46, 9643−9666.

(17) Ricciardulli, A. G.; Yang, S.; Feng, X.; Blom, P. W. M. Solution-Processable High-Quality Graphene for Organic Solar Cells. *ACS Appl. Mater. Interfaces* 2017, 9, 25412−25417.

(18) Pumera, M. Graphene in Biosensing. *Mater. Today* 2011, 14, 308−315.

(19) Zeng, M.; Xiao, Y.; Liu, J.; Lu, W.; Fu, L. Controllable Fabrication of Nanostructured Graphene Towards Electronics. *Adv. Electron Mater.* 2016, 2, No. 1500456.

(20) Yuan, W.; Shi, G. Graphene-Based Gas Sensors. *J. Mater. Chem. A* 2013, 1, 10078.

(21) Basu, S.; Bhattacharyya, P. Recent Developments on Graphene and Graphene Oxide Based Solid State Gas Sensors. *Sens. Actuators, B* 2012, 173, 1−21.

(22) Ricciardella, F.; Vollebregt, S.; Polichetti, T.; Miscuglio, M.; Alfano, B.; Miglietta, M. L.; Massera, E.; Di Francia, G.; Sarro, P. M. Effects of Graphene Defects on Gas Sensing Properties towards NO_2 Detection. *Nanoscale* 2017, 9, 6085−6093.

(23) Prezioso, S.; Perrozzi, F.; Giancaterini, L.; Cantalini, C.; Treossi, E.; Palermo, V.; Nardone, M.; Santucci, S.; Ottaviano, L. Graphene Oxide as a Practical Solution to High Sensitivity Gas Sensing. *J. Phys. Chem. C* 2013, 117, 10683−10690.

(24) Sonda, K.; Kodama, T.; Wea Siga, M. D.; Masumoto, K.; Iwai, M.; Fadil, M.; Ahmad, M. S.; Christopher Agutaya, J. K.; Inomata, Y.; Quitain, A. T.; Hardiansyah, A.; Kida, T. Selective Detection of CO Using Proton-Conducting Graphene Oxide Membranes with Pt-Doped SnO_2 Electrocatalysts: Mechanistic Study by Operando DRIFTS. *ACS Appl. Mater. Interfaces* 2023, 15, 52724−52734.

(25) Guo, L.; Jiang, H.-B.; Shao, R.-Q.; Zhang, Y.-L.; Xie, S.-Y.; Wang, J.-N.; Li, X.-B.; Jiang, F.; Chen, Q.-D.; Zhang, T.; Sun, H.-B. Two-Beam-Laser Interference Mediated Reduction, Patterning and Nanostructuring of Graphene Oxide for the Production of a Flexible Humidity Sensing Device. *Carbon* 2012, 50, 1667−1673.

(26) Gnanaseelan, N.; Marasamy, L.; Mantilla, A.; Kamaraj, S. K.; Espinosa-Faller, F. J.; Caballero-Briones, F. Exploring the Impact of Doping and Co-Doping with B and N on the Properties of Graphene Oxide and Its Photocatalytic Generation of Hydrogen. *Int. J. Hydrogen Energy* 2022, 47, 40905−40919.

(27) Mousavi, H.; Moradian, R. Nitrogen and Boron Doping Effects on the Electrical Conductivity of Graphene and Nanotube. *Solid State Sci.* 2011, 13, 1459−1464.

(28) Matsoso, J. B.; Journet, C.; Coville, N. J.; Sofer, Z. Co-doping Graphene with B and N Heteroatoms for Application in Energy Conversion and Storage Devices. *ChemNanoMat* 2022, 8, No. e202200134.

(29) Deng, X.; Wu, Y.; Dai, J.; Kang, D.; Zhang, D. Electronic Structure Tuning and Band Gap Opening of Graphene by Hole/Electron Codoping. *Phys. Lett. A* 2011, 375, 3890−3894.

(30) Lv, R.; Chen, G.; Li, Q.; McCreary, A.; Botello-Méndez, A.; Morozov, S. V.; Liang, L.; Declerck, X.; Perea-López, N.; Cullen, D. A.; Feng, S.; Elías, A. L.; Cruz-Silva, R.; Fujisawa, K.; Endo, M.; Kang, F.; Charlier, J.-C.; Meunier, V.; Pan, M.; Harutyunyan, A. R.; Novoselov, K. S.; Terrones, M. Ultrasensitive Gas Detection of Large-Area Boron-Doped Graphene. *Proc. Natl. Acad. Sci. U.S.A.* 2015, 112, 14527−14532.

(31) Shaik, M.; Rao, V. K.; Gupta, M.; Murthy, K. S. R. C.; Jain, R. Chemiresistive Gas Sensor for the Sensitive Detection of Nitrogen Dioxide Based on Nitrogen Doped Graphene Nanosheets. *RSC Adv.* 2016, 6, 1527−1534.

(32) Dai, J.; Yuan, J.; Giannozzi, P. Gas Adsorption on Graphene Doped with B, N, Al, and S: A Theoretical Study. *Appl. Phys. Lett.* 2009, 95, No. 232105.

(33) Esrafili, M. D. Boron and Nitrogen Co-Doped Graphene Nanosheets for NO and NO2 Gas Sensing. *Phys. Lett. A* 2019, 383, 1607−1614.

(34) Hummers, W. S.; Offeman, R. E. Preparation of Graphitic Oxide. *J. Am. Chem. Soc.* 1958, 80, 1339.

(35) Muzyka, R.; Kwoka, M.; Smędowski, Ł.; Díez, N.; Gryglewicz, G. Oxidation of Graphite by Different Modified Hummers Methods. *New Carbon Mater.* 2017, 32, 15−20.

(36) Zhou, Y.; Jiang, Y.; Xie, T.; Tai, H.; Xie, G. A Novel Sensing Mechanism for Resistive Gas Sensors Based on Layered Reduced Graphene Oxide Thin Films at Room Temperature. *Sens. Actuators, B* 2014, 203, 135−142.

(37) Dubey, S. P.; Nguyen, T. T. M.; Kwon, Y.-N.; Lee, C. Synthesis and Characterization of Metal-Doped Reduced Graphene Oxide Composites, and Their Application in Removal of *Escherichia Coli*, Arsenic and 4-Nitrophenol. *J. Ind. Eng. Chem.* 2015, 29, 282−288.

(38) Hidayah, N. M. S.; Liu, W.-W.; Lai, C.-W.; Noriman, N. Z.; Khe, C.-S.; Hashim, U.; Lee, H. C. Comparison on Graphite, Graphene Oxide and Reduced Graphene Oxide: Synthesis and Characterization. *AIP Conf. Proc.* 2017, 1892, No. 150002, DOI: 10.1063/1.5005764.

(39) Qian, L.; Thiruppathi, A. R.; van der Zalm, J.; Chen, A. Graphene Oxide-Based Nanomaterials for the Electrochemical Sensing of Isoniazid. *ACS Appl. Nano Mater.* 2021, 4, 3696−3706.

(40) Junaid, M.; Khir, M. H. M.; Witjaksono, G.; Tansu, N.; Saheed, M. S. M.; Kumar, P.; Ullah, Z.; Yar, A.; Usman, F. Boron-Doped Reduced Graphene Oxide with Tunable Bandgap and Enhanced Surface Plasmon Resonance. *Molecules* 2020, 25, 3646.

(41) Duan, X.; Indrawirawan, S.; Sun, H.; Wang, S. Effects of Nitrogen-, Boron-, and Phosphorus-Doping or Codoping on Metal-Free Graphene Catalysis. *Catal. Today* 2015, 249, 184−191.

(42) Stobinski, L.; Lesiak, B.; Malolepszy, A.; Mazurkiewicz, M.; Mierzwa, B.; Zemek, J.; Jiricek, P.; Bieloshapka, I. Graphene Oxide and Reduced Graphene Oxide Studied by the XRD, TEM and Electron Spectroscopy Methods. *J. Electron Spectrosc. Relat. Phenom.* 2014, 195, 145−154.

(43) Agusu, L.; Ahmad, L. O.; Alimin; Nurdin, M.; Herdianto; Mitsudo, S.; Kikuchi, H. Hydrothermal Synthesis of Reduced Graphene Oxide Using Urea as Reduction Agent: Excellent X-Band Electromagnetic Absorption Properties. *IOP Conf. Ser.: Mater. Sci. Eng.* 2018, 367, No. 012002.

(44) Wu, J.-B.; Lin, M.-L.; Cong, X.; Liu, H.-N.; Tan, P.-H. Raman spectroscopy of graphene-based materials and its applications in related devices. *Chem. Soc. Rev.* 2018, 47, 1822−1873.

(45) Pham, P. A Library of Doped-Graphene Images via Transmission Electron Microscopy. *C* 2018, 4, 34.

(46) Tabassum, H.; Zou, R.; Mahmood, A.; Liang, Z.; Guo, S. A Catalyst-Free Synthesis of B, N Co-Doped Graphene Nanostructures with Tunable Dimensions as Highly Efficient Metal Free Dual Electrocatalysts. *J. Mater. Chem. A* 2016, 4, 16469−16475.

(47) Rochman, R. A.; Wahyuningsih, S.; Ramelan, A. H. Preparation of Nitrogen and Sulphur Co-Doped Reduced Graphene Oxide (RGO-NS) Using N and S Heteroatom of Thiourea Preparation of Nitrogen and Sulphur Co-Doped Reduced Graphene Oxide (RGO-NS) Using N and S Heteroatom of Thiourea. *IOP Conf. Ser.: Mater.*

Sci. Eng. **2019**, *509*, No. 012119, DOI: 10.1088/1757-899X/509/1/012119.

(48) Abid; Sehrawat, P.; Islam, S. S.; Mishra, P.; Ahmad, S. Reduced Graphene Oxide (RGO) Based Wideband Optical Sensor and the Role of Temperature, Defect States and Quantum Efficiency. *Sci. Rep.* **2018**, *8*, No. 3537, DOI: 10.1038/s41598-018-21686-2.

(49) Ariharan, A.; Viswanathan, B.; Nandhakumar, V. Nitrogen Doped Graphene as Potential Material for Hydrogen Storage. *Graphene* **2017**, *06*, 41−60.

(50) Rochman, R. A.; Wahyuningsih, S.; Ramelan, A. H.; Hanif, Q. A. Preparation of Nitrogen and Sulphur Co-Doped Reduced Graphene Oxide (RGO-NS) Using N and S Heteroatom of Thiourea. *IOP Conf. Ser.: Mater. Sci. Eng.* **2019**, *509*, No. 012119.

(51) Xiang, Z.; Zhou, X.; Wan, G.; Zhang, G.; Cao, D. Improving Energy Conversion Efficiency of Dye-Sensitized Solar Cells by Modifying TiO_2 Photoanodes with Nitrogen-Reduced Graphene Oxide. *ACS Sustainable Chem. Eng.* **2014**, *2*, 1234−1240.

(52) Ouyang, W.; Zeng, D.; Yu, X.; Xie, F. Exploring the Active Sites of Nitrogen-Doped Graphene as Catalysts for the Oxygen Reduction Reaction ScienceDirect Exploring the Active Sites of Nitrogen-Doped Graphene as Catalysts for the Oxygen Reduction Reaction. *Int. J. Hydrogen Energy* **2014**, *39*, 15996−16005, DOI: 10.1016/j.ijhydene.2014.01.045.

(53) Beams, R.; Gustavo Cançado, L.; Novotny, L. Raman Characterization of Defects and Dopants in Graphene. *J. Phys.: Condens. Matter* **2015**, *27*, No. 083002.

(54) Aunkor, M. T. H.; Mahbubul, I. M.; Saidur, R.; Metselaar, H. S. C. The Green Reduction of Graphene Oxide. *RSC Adv.* **2016**, *6*, 27807−27828.

(55) Ferrari, A. C. Raman Spectroscopy of Graphene and Graphite: Disorder, Electron−Phonon Coupling, Doping and Nonadiabatic Effects. *Solid State Commun.* **2007**, *143*, 47−57.

(56) Ferrari, A. C.; Meyer, J. C.; Scardaci, V.; Casiraghi, C.; Lazzeri, M.; Mauri, F.; Piscanec, S.; Jiang, D.; Novoselov, K. S.; Roth, S.; Geim, A. K. Raman Spectrum of Graphene and Graphene Layers. *Phys. Rev. Lett.* **2006**, *97*, No. 187401.

(57) Tang, Z.-R.; Zhang, Y.; Zhang, N.; Xu, Y.-J. New Insight into the Enhanced Visible Light Photocatalytic Activity over Boron-Doped Reduced Graphene Oxide. *Nanoscale* **2015**, *7*, 7030−7034.

(58) Wang, H.; Maiyalagan, T.; Wang, X. Review on Recent Progress in Nitrogen-Doped Graphene: Synthesis, Characterization, and Its Potential Applications. *ACS Catal.* **2012**, *2*, 781−794.

(59) Johra, F. T.; Lee, J.-W.; Jung, W.-G. Facile and Safe Graphene Preparation on Solution Based Platform. *J. Ind. Eng. Chem.* **2014**, *20*, 2883−2887.

(60) Wang, S.; Feng, J.; Meng, Q.; Cao, B.; Tian, G. Study on Boron and Nitrogen Co-Doped Graphene Xerogel for High-Performance Electrosorption Application. *J. Solid State Electrochem.* **2019**, *23*, 2377−2390.

(61) Mannan, M. A.; Hirano, Y.; Quitain, A. T.; Koinuma, M.; Kida, T. Graphene Oxide to B, N Co-Doped Graphene through Tris-Dimethylaminoborane Complex by Hydrothermal Implantation. *Am. J. Mater. Sci.* **2019**, *9*, 22−28, DOI: 10.5923/j.materials.20190901.04.

(62) Li, S.; Wang, Z.; Jiang, H.; Zhang, L.; Ren, J.; Zheng, M.; Dong, L.; Sun, L. Plasma-Induced Highly Efficient Synthesis of Boron Doped Reduced Graphene Oxide for Supercapacitors. *Chem. Commun.* **2016**, *52*, 10988−10991.

(63) Zhu, T.; Li, S.; Ren, B.; Zhang, L.; Dong, L.; Tan, L. Plasma-Induced Synthesis of Boron and Nitrogen Co-Doped Reduced Graphene Oxide for Super-Capacitors. *J. Mater. Sci.* **2019**, *54*, 9632−9642.

(64) Mkhoyan, K. A.; Contryman, A. W.; Silcox, J.; Stewart, D. A.; Eda, G.; Mattevi, C.; Miller, S.; Chhowalla, M. Atomic and Electronic Structure of Graphene-Oxide. *Nano Lett.* **2009**, *9*, 1058−1063.

(65) Guo, B.; Fang, L.; Zhang, B.; Gong, J. R. Graphene Doping: A Review. *Insci. J.* **2011**, *1*, 80−89.

(66) Yan, W.; Worsley, M. A.; Pham, T.; Zettl, A.; Carraro, C.; Maboudian, R. Effects of Ambient Humidity and Temperature on the NO2 Sensing Characteristics of WS2/Graphene Aerogel. *Appl. Surf. Sci.* **2018**, *450*, 372−379.

(67) Deng, X.; Gao, T.; Dai, J. Temperature Dependence of Adsorption and Desorption Dynamics of NO2Molecule on Boron-Doped Graphene. *Physica E* **2022**, *137*, No. 115083.

(68) Tian, W.; Liu, X.; Yu, W. Research Progress of Gas Sensor Based on Graphene and Its Derivatives: A Review. *Appl. Sci.* **2018**, *8*, 1118.

(69) Schedin, F.; Geim, A. K.; Morozov, S. V.; Hill, E. W.; Blake, P.; Katsnelson, M. I.; Novoselov, K. S. Detection of Individual Gas Molecules Adsorbed on Graphene. *Nat. Mater.* **2007**, *6*, 652−655.

(70) Kacem, K.; Casanova-Chafer, J.; Ameur, S.; Nsib, M. F.; Llobet, E. Gas Sensing Properties of Graphene Oxide Loaded with SrTiO3 Nanoparticles. *J. Alloys Compd.* **2023**, *941*, No. 169011.

(71) Chang, Y.-S.; Chen, F.-K.; Tsai, D.-C.; Kuo, B.-H.; Shieu, F.-S. N-Doped Reduced Graphene Oxide for Room-Temperature NO Gas Sensors. *Sci. Rep.* **2021**, *11*, No. 20719.

(72) Wu, J.; Wu, Z.; Ding, H.; Yang, X.; Wei, Y.; Xiao, M.; Yang, Z.; Yang, B.-R.; Liu, C.; Lu, X.; Qiu, L.; Wang, X. Three-Dimensional-Structured Boron- and Nitrogen-Doped Graphene Hydrogel Enabling High-Sensitivity NO_2 Detection at Room Temperature. *ACS Sens.* **2019**, *4*, 1889−1898.

(73) Li, J.; Lu, Y.; Ye, Q.; Cinke, M.; Han, J.; Meyyappan, M. Carbon Nanotube Sensors for Gas and Organic Vapor Detection. *Nano Lett.* **2003**, *3*, 929−933.

(74) Adjizian, J.-J.; Leghrib, R.; Koos, A. A.; Suarez-Martinez, I.; Crossley, A.; Wagner, P.; Grobert, N.; Llobet, E.; Ewels, C. P. Boron- and Nitrogen-Doped Multi-Wall Carbon Nanotubes for Gas Detection. *Carbon* **2014**, *66*, 662−673.

(75) Fowler, J. D.; Allen, M. J.; Tung, V. C.; Yang, Y.; Kaner, R. B.; Weiller, B. H. Practical Chemical Sensors from Chemically Derived Graphene. *ACS Nano* **2009**, *3*, 301−306.